

# NeuralAnnot: Neural Annotator for in-the-wild Expressive 3D Human Pose and Mesh Training Sets

Gyeongsik Moon

Kyoung Mu Lee

ECE & ASRI, Seoul National University, Korea

{mks0601, kyoungmu}@snu.ac.kr

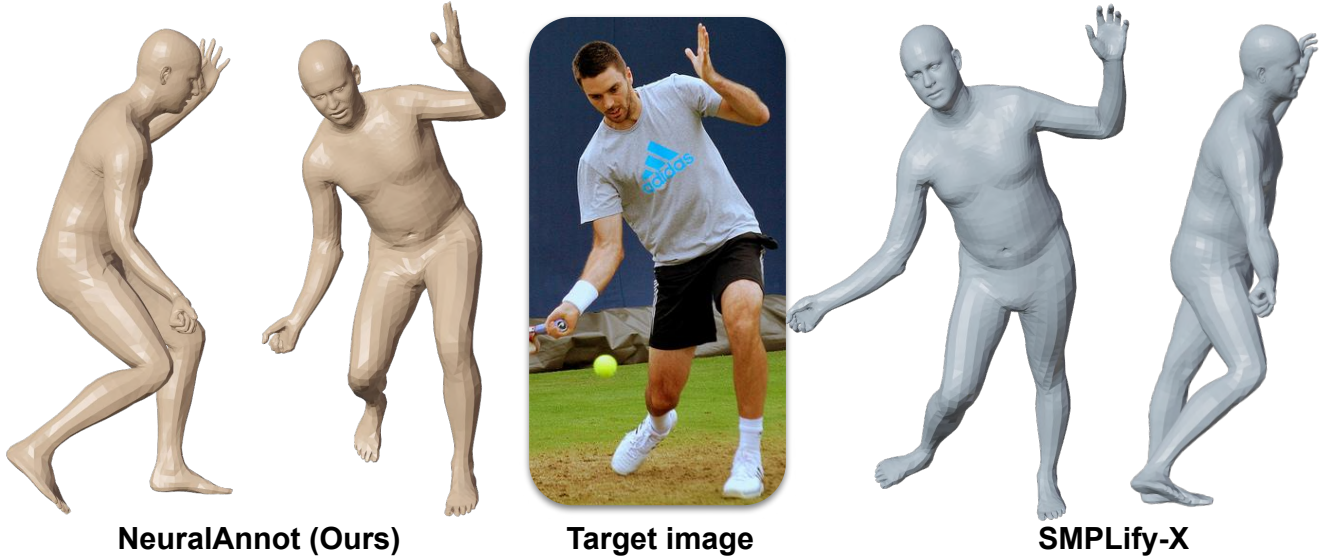


Figure 1: Comparison between pseudo-GT 3D meshes from our NeuralAnnot and an optimization-based method, SMPLify-X [28]. Our NeuralAnnot produces a far better pseudo-GT expressive 3D human mesh with much shorter running time.

## Abstract

Recovering expressive 3D human pose and mesh from in-the-wild images is greatly challenging due to the absence of the training data. Several optimization-based methods have been used to obtain pseudo-groundtruth (GT) 3D poses and meshes from GT 2D poses. However, they often produce bad ones with long running time because their frameworks are optimized on each sample only using 2D supervisions in a sequential way. To overcome the limitations, we present NeuralAnnot, a neural annotator that learns to construct in-the-wild expressive 3D human pose and mesh training sets. Our NeuralAnnot is trained on a large number of samples by 2D supervisions from a target in-the-wild dataset and 3D supervisions from auxiliary datasets with GT 3D poses in a parallel way. We show that our NeuralAnnot produces far better 3D pseudo-GTs with much shorter running time than the optimization-based methods, and the newly obtained training set brings great performance gain. The newly ob-

tained training sets and codes will be publicly available.

## 1. Introduction

Expressive 3D human pose and mesh estimation aims to localize joints and mesh vertices of all human parts, including body, hands, and face, simultaneously in the 3D space. By combining 3D pose and mesh of all human parts, we can understand not only human articulation and shape, but also human intention and feeling, which can be useful in motion capture, virtual/augmented reality, and human action recognition. This is a very challenging task because of the complicated human body and hand articulations and the absence of an in-the-wild training set.

Collecting 3D human pose and mesh data usually requires well-calibrated cameras or markers. However, setting those equipment takes high costs, which makes capturing 3D pose and mesh from daily life at any time and any place very hard. Thus, most of the datasets that provide GT

3D poses and meshes [7, 11, 23, 26, 36] are captured in special environments, such as multi-view studio, which have limited image appearance. Recent 3DPW dataset [32] provides GT 3D poses and meshes from outdoor images; however, the appearance and pose diversity and the data scale are limited due to the difficulty of the capture.

Alternatively, optimization-based methods [3, 28] have been widely used to obtain pseudo-GT 3D poses and meshes from in-the-wild images, used as a training set. They iteratively fit a 3D human model (*e.g.*, SMPL [22] for body, MANO [30] for hands, FLAME [19] for face, or SMPL-X [28] for all parts) to the GT 2D pose of each sample. Although they work well when the target pose is similar to the initial one and has a small depth ambiguity, such as 3D face fitting, they often produce inaccurate and implausible pseudo-GT 3D body/hand poses and meshes, as shown in Figure 1. Also, they suffer from a long running time. The first reason for the failure is that they sequentially optimize their frameworks on each sample, thus takes a large amount of time and can be easily stuck in local minima. Second, their frameworks are optimized using only 2D supervisions and heavily rely on prior terms to prevent implausible poses. Complicated articulations of the human body and hand make the optimization hard without using 3D supervisions.

To overcome the limitations of the optimization-based methods, we present *NeuralAnnot*, a neural annotator that learns to construct in-the-wild expressive 3D human pose and mesh training sets. Unlike the optimization-based methods that sequentially optimize their frameworks on each sample, our *NeuralAnnot* is trained on a large number of samples in a parallel way. Therefore, *NeuralAnnot* takes a much shorter running time while it is much more robust to the local minima. In addition, our *NeuralAnnot* is jointly trained using 2D supervisions from a target in-the-wild dataset and 3D supervisions from auxiliary datasets that have GT 3D poses. The 2D supervisions from a target in-the-wild dataset make *NeuralAnnot* generalize well to diverse image appearance; however, relying only on 2D supervision can make the system suffer from severe depth ambiguity. On the other hand, the 3D supervisions from the auxiliary datasets make *NeuralAnnot* accurately predict 3D pose and mesh; however, relying only on 3D supervisions from the auxiliary datasets can make the system not generalize well to diverse image appearances because the datasets with GT 3D poses are usually captured from restricted lab environments. Our *NeuralAnnot* takes the strong points of both 2D and 3D supervisions by the joint training, making it output much accurate and plausible pseudo-GT 3D poses and meshes.

Our *NeuralAnnot* takes a single RGB image and outputs 3D human model parameters [22, 28, 30], which becomes a new pseudo-GT of the input image. For the supervision,

it only requires GT 2D or 3D pose of the datasets without any prepared 3D human model fits. We use *NeuralAnnot* to obtain pseudo-GT expressive 3D human pose and mesh from in-the-wild dataset [8, 20], which severs a highly useful training set. Figure 1 shows comparison between obtained pseudo-GT 3D meshes from *NeuralAnnot* and previous widely used optimization-based method, SMPLify-X [28]. We will release the newly obtained pseudo-GTs and codes for the continual study of expressive 3D human pose and mesh estimation in the wild. In addition, we will apply *NeuralAnnot* to most of the existing human body/hand/face datasets [1, 2, 7, 9, 15, 20, 23, 24, 26, 32, 37] and release all pseudo-GTs.

Our contributions can be summarized as follows.

- We present *NeuralAnnot*, a neural annotator that learns to construct in-the-wild expressive 3D human pose and mesh training sets. Our *NeuralAnnot* is trained on a large number of samples in a parallel way with 2D and 3D supervisions.
- Our *NeuralAnnot* produces far better 3D pseudo-GTs with much shorter running time than previous optimization-based methods, and the newly obtained training set brings great performance gain.
- The newly obtained pseudo-GT expressive and part-specific 3D human poses and meshes will be publicly released. We believe the new pseudo-GTs will be highly beneficial to the community.

## 2. Related works

**Expressive 3D human pose and mesh estimation.** Although there have been many attempts to recover part-specific 3D human pose and mesh [14, 17, 25, 29], there have been very few attempts to simultaneously recover the 3D human pose and mesh of all human parts, including body, hands, and face, because of its difficulty. Most of the previous attempts are optimization-based the approach, which fits a 3D human model to the 2D/3D evidence. Joo *et al.* [13] fits their human models to 3D human joints coordinates and point clouds in a multi-view studio environment. Xiang *et al.* [33] extended Joo *et al.* [13] to the single RGB case. Pavlakos *et al.* [28] and Xu *et al.* [35] fits their human model, SMPL-X and GHUM, respectively, to 2D human joint coordinates. As the above optimization-based methods can be slow and prone to noisy evidence, a regression-based approach is presented recently. Choutas *et al.* [5] presented ExPose, which predicts the expressive human pose and mesh using body-driven attention.

Our *NeuralAnnot* can be categorized into the regression-based approach and has clear differences compared with

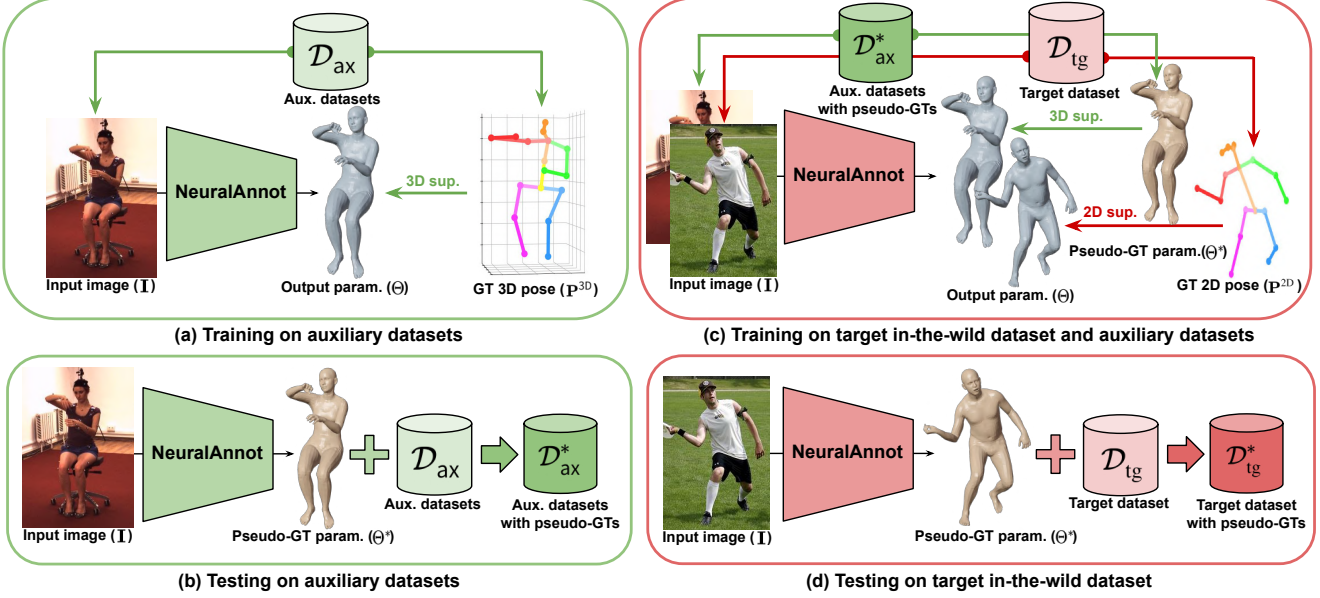


Figure 2: Overall pipeline of NeuralAnnot. (a) We first train NeuralAnnot on the auxiliary datasets that provide GT 3D pose. (b) After the training, testing results on the auxiliary datasets becomes pseudo-GTs of the datasets. (c) Another NeuralAnnot is jointly trained on the auxiliary datasets with the pseudo-GTs and the target in-the-wild dataset. (d) After the training, testing results on the target in-the-wild dataset becomes pseudo-GTs of the dataset.

the previous methods. The previous regression-based methods [5] require prepared 3D human model fits [28], used as pseudo-GTs for the training. The optimization-based methods [3, 28] are used to obtain the pseudo-GTs; however, it takes a very large amount of time and often produces bad ones. In contrast, ours do not require the prepared fits, and we use our NeuralAnnot to obtain the pseudo-GTs by replacing the optimization-based methods. The goal of the previous methods and ours is also different. The previous regression-based methods aim to output accurate 3D human pose and mesh on unseen test images, while ours aims to output accurate 3D human pose and mesh on the seen training images.

#### Pseudo-GT 3D pose and mesh from in-the-wild images.

The optimization-based methods, such as SMPLify [3] and SMPLify-X [28], are widely used to obtain pseudo-GT 3D poses and meshes. SMPLify [3] fits a 3D human body model (*i.e.*, SMPL [22]) to a given 2D pose by minimizing 2D pose loss and several prior terms. SMPLify-X [28] is in a similar spirit of SMPLify, and they extended SMPLify for the expressive 3D human model fitting by proposing a new expressive 3D human model, SMPL-X. Although they perform well when the target 2D pose is similar to the initial T-pose of SMPL or SMPL-X, they often output inaccurate and implausible poses when the target pose is far from the initial pose. In addition, they take long running time because they optimize their framework on each sample.

Recently, EFT [12] is introduced to obtain pseudo-GT 3D human body pose and mesh from in-the-wild images. Given a pre-trained 3D human body mesh estimation net-

work [17], they fine-tune the network to GT 2D pose of each training image. However, EFT assumes a well-performing pre-trained 3D human body pose and mesh estimation network is available, which is not applicable to expressive 3D human pose and mesh estimation as only several recent methods [5] have been proposed to address this problem. In addition, preparing pre-trained 3D human body pose and mesh estimation networks requires pseudo-GT 3D pose and mesh to train the network. As the pseudo-GT 3D poses and meshes are usually obtained by the optimization-based methods [3, 28], it takes a large amount of time.

Compared with the above approaches [3, 12, 28], our NeuralAnnot has clear novel and strong points. First, it is much more robust to the local minima and much faster than the above methods because ours is trained and tested on a large number of samples in a parallel way, while the above methods require a sequential sample-specific optimization. Second, it gets benefits from 3D supervisions using auxiliary datasets that provide GT 3D pose, while others only rely on 2D supervisions when obtaining pseudo-GTs. Third, it does not require prepared pseudo-GT 3D pose and mesh to train networks, which can save great efforts, while EFT [12] requires.

### 3. NeuralAnnot

We design NeuralAnnot as a simple combination of ResNet [6] and a regressor, which extracts image feature vector  $\mathbf{F}$  and regresses a set of 3D human model parameters  $\Theta$ , respectively.  $\mathbf{F}$  is obtained by performing global av-

---

**Algorithm 1** Neural annotation

---

**Input:**  $\mathcal{D}_{\text{ax}}$ : Auxiliary datasets with GT 3D pose  
**Input:**  $\mathcal{D}_{\text{tg}}$ : Target in-the-wild dataset with GT 2D pose  
**Output:**  $\mathcal{D}_{\text{ax}}^*$ :  $\mathcal{D}_{\text{ax}}$  and predicted pseudo-GTs  
**Output:**  $\mathcal{D}_{\text{tg}}^*$ :  $\mathcal{D}_{\text{tg}}$  and predicted pseudo-GTs

- 1: **for**  $n \leftarrow 1$  to  $N_{\text{ax}}$  **do**
- 2:   Randomly initialize NeuralAnnot
- 3:   Train NeuralAnnot on  $\mathcal{D}_{\text{ax},n}$  by minimizing  $L_{\text{ax}}$
- 4:   Test NeuralAnnot on all images of  $\mathcal{D}_{\text{ax},n}$
- 5:    $\mathcal{D}_{\text{ax},n}^* = \{D \cap \Theta^* | D \in \mathcal{D}_{\text{ax},n}\}$
- 6: **end for**
- 7: Randomly initialize NeuralAnnot
- 8: Train NeuralAnnot on  $\mathcal{D}_{\text{tg}}$  and  $\mathcal{D}_{\text{ax}}^*$  by minimizing  $L_{\text{tg}}$
- 9: Test NeuralAnnot on all images of  $\mathcal{D}_{\text{tg}}$
- 10:  $\mathcal{D}_{\text{tg}}^* = \{D \cap \Theta^* | D \in \mathcal{D}_{\text{tg}}\}$

---

erage pooling on the ResNet output feature. The regressor consists of several fully connected layers, and the 3D human model parameter set is different for each human model, which will be described in Section 4. The 3D human pose and mesh can be obtained from  $\Theta$  using 3D human models [19, 22, 28, 30].

The procedure of the neural annotation is described in Algorithm 1. NeuralAnnot is jointly trained on a target in-the-wild dataset with GT 2D pose  $\mathcal{D}_{\text{tg}} = \{(\mathbf{I}_n, \mathbf{P}_n^{2D})\}_{n=1}^{N_{\text{tg}}}$  and auxiliary datasets with GT 3D pose  $\mathcal{D}_{\text{ax}} = \{\mathcal{D}_{\text{ax},n}\}_{n=1}^{N_{\text{ax}}}$ , where  $\mathcal{D}_{\text{ax},\bullet} = \{(\mathbf{I}_n, \mathbf{P}_n^{2D}, \mathbf{P}_n^{3D})\}_{n=1}^{N_{\text{ax},\bullet}}$ .  $\mathbf{I}$ ,  $\mathbf{P}^{2D}$ ,  $\mathbf{P}^{3D}$ , and  $N$  denote image, GT 2D pose, GT 3D pose, and the number of samples, respectively. To this end, we first obtain pseudo-GT 3D human model parameters of the auxiliary datasets, thus  $\mathcal{D}_{\text{ax}}$  becomes  $\mathcal{D}_{\text{ax}}^* = \{\mathcal{D}_{\text{ax},n}^*\}_{n=1}^{N_{\text{ax}}}$ , where  $\mathcal{D}_{\text{ax},\bullet}^* = \{D \cap \Theta^* | D \in \mathcal{D}_{\text{ax},\bullet}\}$ . Then, the auxiliary datasets with the obtained pseudo-GTs  $\mathcal{D}_{\text{ax}}^*$  are used to obtain pseudo-GT 3D human model parameters of the target in-the-wild dataset, thus  $\mathcal{D}_{\text{tg}}$  becomes  $\mathcal{D}_{\text{tg}}^* = \{D \cap \Theta^* | D \in \mathcal{D}_{\text{tg}}\}$ , as shown in Figure 2.  $\cap$  and  $\Theta^*$  denote tuple extension<sup>1</sup> and predicted 3D human model parameters from  $\mathbf{I}$  in  $D$  after the training, which is a new pseudo-GT, respectively. We provide detailed descriptions of how to obtain pseudo-GT 3D human pose and mesh from the auxiliary and target datasets below.

### 3.1. Pseudo-GTs of datasets with GT 3D pose

The regressor takes a pair of image feature  $\mathbf{F}$  and GT 3D pose  $\mathbf{P}^{3D}$  when NeuralAnnot is trained to predict pseudo-GTs of the auxiliary datasets that provide GT 3D pose  $\mathcal{D}_{\text{ax}}$  [7, 23, 26]. The image feature provides human articulation and shape information, while GT 3D pose additionally provides depth and real scale information, which lacks in the 2D image feature. To this end, the GT 3D pose  $\mathbf{P}^{3D}$  is converted to a 512-dimensional feature by two fully con-

nected layers and concatenated with global average pooled ResNet output feature  $\mathbf{F}$ . The concatenated feature is fed to a fully connected layer for the 3D human model parameter regression. The 3D rotations of joints in the predicted 3D human model parameters are initially predicted in a 6D rotational representation of Zhou *et al.* [38] and converted to a 3D axis-angle rotation. The loss function is defined as follows:

$$L_{\text{ax}} = \|\hat{\mathbf{P}}^{3D} - \mathbf{P}^{3D}\|_1 + \lambda_{\text{ax}} \sum_{\theta \in \Theta} \hat{\theta}^2,$$

where the hat mark indicates a predicted output.  $\hat{\mathbf{P}}^{3D}$  is obtained from 3D human model layer.  $\lambda_{\text{ax},\theta}$  denotes  $L2$  norm regularizer weight of each 3D human parameter  $\theta$ . After the training, the testing results on all images of the dataset become new pseudo-GTs of the dataset, which form  $\mathcal{D}_{\text{ax},\bullet}^*$ .

### 3.2. Pseudo-GTs of datasets without GT 3D pose

The regressor outputs 3D human model parameters from the image feature  $\mathbf{F}$  when NeuralAnnot is trained to predict pseudo-GTs of in-the-wild datasets that do not provide GT 3D pose  $\mathcal{D}_{\text{tg}}$  [20]. The most important contribution of our NeuralAnnot is that we use the auxiliary datasets with the obtained pseudo-GTs  $\mathcal{D}_{\text{ax}}^*$  for the pseudo-GTs of a target in-the-wild dataset  $\mathcal{D}_{\text{tg}}$ . To this end, we make a mini-batch of each iteration from multiple datasets, including the auxiliary datasets  $\mathcal{D}_{\text{ax}}^*$  and the target in-the-wild dataset  $\mathcal{D}_{\text{tg}}$ . Thus, our NeuralAnnot is jointly trained on the auxiliary datasets and target in-the-wild dataset and can benefit from the strong 3D supervisions from the auxiliary datasets.

Although samples from the auxiliary datasets can benefit NeuralAnnot by the strong 3D supervisions, samples from the target in-the-wild datasets are supervised only using GT 2D pose. To prevent implausible 3D human pose and mesh induced by the 2D supervisions, NeuralAnnot predicts a low-dimensional embedding of the 3D rotations (*i.e.*, a latent code of VPoser [28] for the body part and PCA coefficients for the hand part [30]) unlike directly predicting 3D rotations when trained to output pseudo-GTs of the auxiliary datasets  $\mathcal{D}_{\text{ax}}$ . The low-dimensional embedding can effectively limit the 3D human pose and mesh to plausible articulation space, thus can prevent implausible 3D human pose and mesh. Note that the low-dimensional embeddings can be learned from  $\mathcal{D}_{\text{ax}}^*$ , if not available. The loss function is defined as follows:

$$L_{\text{tg}} = \|\hat{\mathbf{P}}^{2D} - \mathbf{P}^{2D}\|_1 + \mathbb{1}_{\text{tg}} \lambda_{\text{tg}} \sum_{\theta \in \Theta} \hat{\theta}^2 + (1 - \mathbb{1}_{\text{tg}}) (\|\hat{\mathbf{P}}^{3D} - \mathbf{P}^{3D}\|_1 + \sum_{\theta \in \Theta} \|\hat{\theta} - \theta^*\|_1),$$

where the hat mark indicates a predicted output.  $\theta^*$  is from  $\Theta^*$ .  $\lambda_{\text{tg},\theta}$  denotes  $L2$  norm regularizer weight of each 3D

---

<sup>1</sup> $(a, b) \cap c = (a, b, c)$



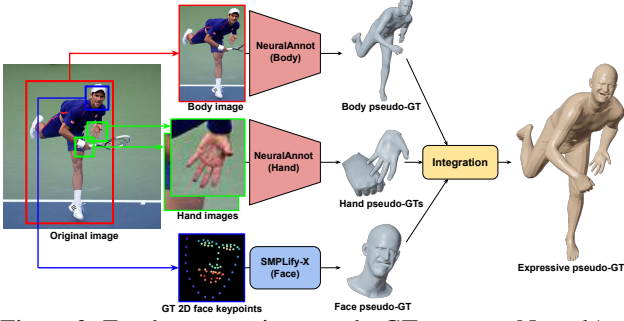


Figure 3: For the expressive pseudo-GTs, we use NeuralAnnot for the body and hand parts, and SMPLify-X [28] for the face part. The integration module integrates part-specific pseudo-GTs to an expressive pseudo-GT.

human model parameter  $\theta$  for samples from the target in-the-wild dataset.  $\mathbb{1}_{\text{tg}}$  is 1 when a sample is from target in-the-wild dataset  $\mathcal{D}_{\text{tg}}$  and zero otherwise. After the training, the testing results on all images of the target in-the-wild dataset become new pseudo-GTs of the dataset, which form  $\mathcal{D}_{\text{tg}}^*$ .

#### 4. Expressive 3D human pose and mesh train sets

For the pseudo-GT expressive 3D human pose and mesh, we design separated networks for the body and hand parts following Choutas *et al.* [5], as shown in Figure 3. This separation enables us to use part-specific datasets, such as Human3.6M [7] and FreiHAND [39]. For the face, we use SMPLify-X [28] to obtain pseudo-GT 3D face model parameter instead of using NeuralAnnot because not complicated articulations of the face make SMPLify-X work well. After obtaining pseudo-GTs of body, hand, and face parts, an integration module integrates part-specific pseudo-GTs to expressive pseudo-GTs, which will be described in the following subsections.

##### 4.1. Body part

The body part network predicts SMPL-X parameters, including 3D body global rotation  $\theta_b^g \in \mathbb{R}^3$ , 3D body rotations  $\theta_b \in \mathbb{R}^{21 \times 3}$ , shape parameter  $\beta_b \in \mathbb{R}^{10}$ , and camera parameter  $k_b \in \mathbb{R}^3$ . We set  $\Theta = \{\theta_b, \beta_b\}$  and  $\Theta = \{z_b, \beta_b\}$  when training NeuralAnnot to minimize  $L_{\text{ax}}$  and  $L_{\text{tg}}$ , respectively.  $z_b$  denotes the latent code of the VPoser [28].

##### 4.2. Hand part

The hand part outputs MANO parameters, including 3D hand global rotation  $\theta_h^g \in \mathbb{R}^3$ , 3D hand rotations  $\theta_h \in \mathbb{R}^{15 \times 3}$ , shape parameter  $\beta_h \in \mathbb{R}^{10}$ , and camera parameter  $k_h \in \mathbb{R}^3$ . We set  $\Theta = \{\theta_h, \beta_h\}$  and  $\Theta = \{z_h, \beta_h\}$  when training NeuralAnnot to minimize  $L_{\text{ax}}$  and  $L_{\text{tg}}$ , respectively.  $z_h$  denotes the 3D hand pose PCA coefficients, defined in MANO.

#### 4.3. Face part

We modified SMPLify-X to fit FLAME on GT 2D face keypoints. The original loss functions, including keypoint loss and a set of priors, are used for the fitting. It optimizes 3D face global rotation  $\theta_f^g \in \mathbb{R}^3$ , 3D jaw rotation  $\theta_f \in \mathbb{R}^3$ , shape parameter  $\beta_f \in \mathbb{R}^{10}$ , and expression code  $\psi \in \mathbb{R}^{10}$ .

#### 4.4. Integration of all parts after the training

After obtaining the part-specific pseudo-GTs, the final pseudo-GT expressive 3D human poses and meshes are obtained by forwarding  $\{\theta_b^g, \theta_b, \beta_b, \theta_{rh}^g, \theta_{rh}, \theta_{lh}^g, \theta_{lh}, \theta_f, \psi\}$  to SMPL-X, where  $*_{rh}$  and  $*_{lh}$  denote  $*$  is from right and left hand, respectively. The 3D hand pose parameter  $\theta_h$  of MANO and 3D jaw rotation  $\theta_f$  and face expression code  $\psi$  of FLAME are compatible with those of SMPL-X; thus, we use them for the final prediction. As the body part often predicts wrong rotations of elbows and wrists in the roll axis, we selectively use the 3D hand global rotation  $\theta_h^g$  to replace rotations of the elbows and wrists based on a simple thresholding. The thresholding assumes rotations of elbows and wrists in the roll axis are almost the same, which follows the anatomical structure of the human body. We provide detailed descriptions of the thresholding in the supplementary material.

#### 5. Implementation details

PyTorch [27] is used for implementation. The backbone part is initialized with the publicly released ResNet50 [6] pre-trained on ImageNet [31]. The weights are updated by the Adam optimizer [16] with a mini-batch size of 192. Each mini-batch consists of half samples from the auxiliary datasets and half samples from the target in-the-wild dataset. All input images are cropped using groundtruth box and resized to  $256 \times 256$ . No data augmentation is performed. The initial learning rate is set to  $10^{-4}$  and reduced by a factor of 10 when it converges. We train body and hand parts separately with four NVIDIA RTX 2080 Ti GPUs. All the other hyperparameters will be available in the released codes.

#### 6. Experiment

##### 6.1. Datasets and evaluation metrics.

**Datasets.** For the body part, we use Human3.6M [7], MPI-INF-3DHP [23], and 3DPW [32] as the auxiliary datasets. For the hand part, FreiHAND [39] and InterHand2.6M [26] are used as the auxiliary dataset. For both parts, we use the whole-body version of MSCOCO [8, 20] as the target in-the-wild dataset. For the face part, we run SMPLify-X [28] on MSCOCO whole-body version [8] and FFHQ [15]. The expressive 3D human pose and mesh pseudo-GTs are obtained by integrating part-specific ones of MSCOCO [8, 20].

**Evaluation metrics.** There are direct and indirect evaluation metrics. For the direct evaluation, we report 3D annotation error and annotation time. The 3D annotation error is defined as the average 3D joint distance ( $mm$ ) between 3D poses from GTs of the dataset and the pseudo-GTs. The annotation time represents how much time is required for the annotation. When measuring the annotation time of the optimization-based annotators [3, 28], we divide the total samples into four chunks and run the annotators on four separated GPUs as we use four GPUs to train NeuralAnnot.

The absence of the GT 3D pose of the in-the-wild datasets makes calculating the 3D annotation error impossible. Alternatively, we train a 3D human pose and mesh estimator on the obtained pseudo-GTs of the target in-the-wild dataset and use the evaluation results on existing benchmarks as the indirect evaluation metric. The indirect evaluation metric represents how much the pseudo-GTs are beneficial for the training. For the body and hand part analysis, I2L-MeshNet [25] is used as the estimator and evaluated on 3DPW [32] and FreiHAND [39], respectively. We split the FreiHAND training set into training and validation sets and report the results on the validation set. For the all parts analysis, we train a regressor that has the same architecture with NeuralAnnot and evaluate it on EHF [28]. We provide more analysis using different estimators in the supplementary material.

The error of the estimator is measured using the most widely used metrics, MPJPE and MPVPE, where each calculates the average 3D joint distance ( $mm$ ) and 3D mesh vertex distance ( $mm$ ) between predicted and groundtruth, respectively, after a root joint translation alignment. PA MPJPE and PA MPVPE further align a rotation and scale. Area under curve (AUC) is additionally used for the hand part evaluation. In Section 6.2 and 6.3, we use only MeshNet part of the I2L-MeshNet and supervise it only with pseudo-GTs without GT 2D pose of the target dataset. The full I2L-MeshNet with full loss functions is used in Section 6.4.

## 6.2. Ablation study

**Effectiveness of 3D supervisions from the auxiliary datasets.** We show the benefit of the 3D supervisions from the auxiliary datasets in Table 1 using the indirect evaluation metric, introduced in Section 6.1. For each row of the table, NeuralAnnot uses the auxiliary datasets of each row and outputs pseudo-GTs of the target dataset following Algorithm 1. Then, we train I2L-MeshNet [25] on the obtained pseudo-GTs of the target dataset and test on an evaluation set. 3DPW and FreiHAND are used for the evaluation set of the body and hand parts, respectively. The performance of the I2L-MeshNet becomes better when the auxiliary datasets become available, which shows the obtained pseudo-GTs from the NeuralAnnot become more beneficial

Auxiliary datasets	Target dataset	Estimator	Metrics
<b>Human body part</b>			<b>PA MPJPE</b>
None			69.6
Human3.6M [7]	MSCOCO [8, 20]	I2L-MeshNet [25]	66.1
3DPW [32]			68.0
MPI-INF-3DHP [23]			65.9
<b>All (Ours)</b>			<b>64.9</b>
<b>Human hand part</b>			<b>AUC</b>
None			0.758
FreiHAND [39]	MSCOCO [8, 20]	I2L-MeshNet [25]	0.779
InterHand2.6M [26]			0.772
<b>All (Ours)</b>			<b>0.780</b>

Table 1: PA MPJPE and AUC comparison between I2L-MeshNets trained on various pseudo-GTs of body part and hand part MSCOCO, respectively.

Settings	2D error	Estimator	PA MPJPE
wo. VPoser	<b>5.0</b>	I2L-MeshNet	113.5
<b>w. VPoser (Ours)</b>	8.1	[25]	<b>65.9</b>

Table 2: The 2D annotation error (pixel) comparison between various settings of NeuralAnnot on MSCOCO and PA MPJPE comparison between I2L-MeshNets trained on various pseudo-GTs of MSCOCO.

when the 3D supervisions from the auxiliary datasets are used. By using all auxiliary datasets, the performance of the I2L-MeshNet is further improved, which means the pseudo-GTs from the NeuralAnnot becomes more beneficial. The comparisons clearly show the benefit of the 3D supervisions from the auxiliary datasets when training NeuralAnnot.

**Effectiveness of the low-dimensional embedded pose prediction.** We show the benefit of predicting low-dimensional embedded pose (*i.e.*, the latent code of VPoser for the body part) when minimizing  $L_{tg}$  in Table 2 using the indirect evaluation metric, introduced in Section 6.1. To this end, we train I2L-MeshNet on pseudo-GTs obtained by NeuralAnnot of each row of the table and test on 3DPW. For all settings, MPI-INF-3DHP is used as the auxiliary dataset. As the table shows, I2L-MeshNet trained on pseudo-GTs obtained from the low-dimensional pose achieves significant low error, although the pseudo-GTs have higher 2D annotation error. We observed that the low-dimensional pose can effectively prevent implausible poses with very simple regularizers (*i.e.*,  $L_2$  regularizer for ours); thus, it makes the system less suffer from the depth ambiguity. When VPoser is not used, the pose is initially predicted in a 6D rotational representation [38] and converted to the 3D axis-angle following [17]. The 2D annotation error is a pixel distance between GT 2D pose and 2D pose from the pseudo-GTs. The same tendency was observed for the hand part by predicting the PCA coefficients of the hand pose space.



Figure 4: Visualized pseudo-GTs of MSCOCO (first row) and InterHand2.6M (second row).

Datasets	SMPLify-X [28]		NeuralAnnot (Ours)	
	Error	Time	Error	Time
<b>Human body part</b>				
Human3.6M [7]	13.1	12 days	<b>9.8</b>	<b>7 hours</b>
MPI-INF-3DHP [23]	17.9	5 days	<b>16.4</b>	<b>3 hours</b>
<b>Human hand part</b>				
InterHand2.6M [26]	10.0	3 days	<b>5.8</b>	<b>2 hours</b>

Table 3: The 3D annotation error ( $mm$ ) and annotation time comparison between SMPLify-X and our NeuralAnnot on various datasets. GT 3D pose is used for the annotation.

### 6.3. Comparison with previous annotators

**Pseudo-GTs from GT 3D pose.** Table 3 shows the 3D annotation error ( $mm$ ) and annotation time comparison between SMPLify-X [28] and our NeuralAnnot on various datasets that provide GT 3D pose. Both annotates pseudo-GT 3D human model parameters using the GT 3D pose of the dataset. As the table shows, our NeuralAnnot can annotate pseudo-GT 3D human model parameters about *40 times faster* than the previous optimization-based method, SMPLify-X, with the *lower 3D annotation error*. The faster annotation time is from the parallel training and testing, while SMPLify-X sequentially optimizes their framework on each sample. Moreover, the lower 3D annotation error is from the training on a large number of samples, which makes NeuralAnnot more robust to noisy GT 3D poses and local minima compared with sample-specific optimization of the SMPLify-X. The comparisons clearly show the effectiveness of the proposed NeuralAnnot. For the annotation, we ran SMPLify-X and NeuralAnnot on only one view. The 2D/3D coordinates of other views can be automatically obtained by applying the camera parameters, provided in the dataset.

**Pseudo-GTs from GT 2D pose.** We compare our NeuralAnnot with previous annotators in Table 4 using the indirect evaluation metric, introduced in Section 6.1. For this, I2L-MeshNet is trained on pseudo-GTs of MSCOCO,

Annotators	Err.	Time	Estimator	Metrics
<b>Human body part</b>				<b>PA MPJPE</b>
SMPLify [3]	6.9	N/A	I2L-MeshNet [25]	81.7
EFT [12]	5.7	30 days		69.0
SMPLify-X [28]	<b>4.1</b>	6 days		72.7
SMPLify-X* [28]	<b>4.1</b>	10 days		71.8
<b>NeuralAnnot (Ours)</b>	5.2	<b>2 days</b>		<b>67.0</b>
<b>NeuralAnnot* (Ours)</b>	6.5	<b>2 days</b>		<b>64.9</b>
<b>Human hand part</b>				<b>AUC</b>
SMPLify-X [28]	<b>6.4</b>	4 days	I2L-MeshNet [25]	0.741
<b>NeuralAnnot (Ours)</b>	12.5	<b>9 hours</b>		<b>0.780</b>

Table 4: The 2D annotation error (pixel) and annotation time comparison between various annotators on MSCOCO and PA MPJPE comparison between I2L-MeshNets trained on various pseudo-GTs of MSCOCO. The body annotators with \* output pseudo-GTs of all samples in MSCOCO, while without \* output samples only used in EFT.

obtained from each annotator, and tested on 3DPW and FreiHAND for the body and hand part, respectively. As the table shows, I2L-MeshNet trained on pseudo-GTs from our NeuralAnnot achieves significantly better performance compared with I2L-MeshNets trained on pseudo-GTs from other annotators. In addition, our NeuralAnnot requires the shortest annotation time. The comparisons show that pseudo-GTs from our NeuralAnnot is the most beneficial one for the training. The strengths are from parallel training on the large number of samples with 3D supervisions from the auxiliary datasets, discussed in Table 1 and 3, while other annotators perform sequential optimization for each sample. Interestingly, SMPLify-X achieves a smaller 2D annotation error compared with NeuralAnnot, while I2L-MeshNet trained on it performs worse. This shows pseudo-GTs of SMPLify-X suffer from depth ambiguity because it relies on only 2D supervisions for the annotation. We resolve this issue by using 3D supervisions from the auxiliary datasets. The comparisons clearly show the effectiveness of



Annotators	Err.	Time	Estimator	PA MPJPE
<b>NeuralAnnot (Ours)</b>	8.1	<b>2 days</b>		65.9
SMPLify-X on ours	<b>1.1</b>	7 days	I2L-MeshNet	78.2
EFT on ours	7.7	3 days	[25]	65.8
3D sup. on MSCOCO	6.2	12 days		<b>64.6</b>

Table 5: The 2D annotation error (pixel) and annotation time comparison between various annotators on MSCOCO and PA MPJPE comparison between I2L-MeshNets trained on various pseudo-GTs of MSCOCO.

the proposed NeuralAnnot over previous pseudo-GT annotators.

We used SMPLify [3] results released by Kolotouros *et al.* [17]. As they did not report the optimization time, we could not report it; however, we think it may take a similar amount of time with that of SMPLify-X [28] because both are based on a similar optimization framework. We used official released EFT [12] results. The EFT fine-tunes pre-trained SPIN [17] on each training sample. As SPIN uses pseudo-GT SMPL fits of Human3.6M, MPI-INF-3DHP, MSCOCO, MPII [2], and LSP [9, 10] for the training, we calculated the annotation time of the EFT by a summation of 1) SMPLify-X optimization time on the datasets for the pseudo-GTs, 2) training time of SPIN, and 3) sample-specific fine-tuning. Each step takes 12+5+6+4+1 days, 2 days, and several hours, respectively. SMPLify-X optimizes the latent code of VPoser and PCA coefficients for the body and hand part, respectively, like our NeuralAnnot. The annotation time of NeuralAnnot is a total time of Algorithm 1, which includes the annotation time of the auxiliary datasets and the target dataset. The 2D annotation error is a pixel distance between GT 2D pose and 2D pose from the pseudo-GTs.

**Combination with previous annotators.** Table 5 shows how pseudo-GTs of NeuralAnnot changes when combined with previous annotators using the indirect evaluation metric, introduced in Section 6.1. To this end, we trained I2L-MeshNet on pseudo-GTs of MSCOCO, obtained from each annotator, and tested on 3DPW. The pseudo-GTs of the second row (SMPLify-X on ours) are obtained by setting initial values of SMPLify-X to the outputs of NeuralAnnot and running SMPLify-X, similar to the fitting-in-the-loop of SPIN [17]. Following SPIN [17], we used only the last optimization stage of SMPLify-X. The pseudo-GTs of the third row (EFT on ours) are obtained by performing the exemplar fine-tuning [12] using a pre-trained NeuralAnnot. Finally, the pseudo-GTs of the last row (3D sup. on MSCOCO) are obtained by applying 3D supervisions on samples from MSCOCO using pseudo-GTs, obtained by SMPLify-X, when NeuralAnnot is trained to minimize  $L_{\text{fig}}$ . For all settings, MPI-INF-3DHP is used as the auxiliary dataset, and its pseudo-GTs are obtained by NeuralAnnot.

As the table shows, combining previous annotators do

Methods	Pseudo-GTs from	MPJPE	PA MPJPE
HMR [14]	Mosh [21]	130.0	81.3
GraphCMR [18]	Mosh [21]	-	70.2
SPIN [17]	Mosh [21]+SMPLify [3]	96.9	59.2
ExPose [5]	SMPLify-X [28]	93.4	60.7
Pose2Mesh [4]	SMPLify-X [28]	88.9	58.3
I2L-MeshNet [25]	SMPLify-X [28]	93.2	57.7
	<b>NeuralAnnot (Ours)</b>	<b>86.6</b>	<b>54.3</b>

Table 6: MPJPE and PA MPJPE comparison on 3DPW.

Methods	PA MPVPE			PA MPJPE	
	All	Hands	Face	Body	Hands
SMPLify-X [28]	65.3	12.3	6.3	87.6	12.9
MTC [33]	67.2	-	-	107.8	16.7
ExPose [5]	54.5	12.8	5.8	62.8	13.1
<b>Regressor (Ours)</b>	<b>53.5</b>	<b>12.0</b>	<b>5.7</b>	<b>61.4</b>	<b>11.7</b>

Table 7: PA MPVPE and PA MPJPE comparison on EHF. The numbers in hands are averaged values of left and right hands.

not bring significant performance gain to the estimator, while requiring longer annotation time. Especially, combining with SMPLify-X makes the annotation time very long because of the sample-specific sequential optimization. The comparisons show that the pseudo-GTs from our NeuralAnnot are already highly beneficial; thus, NeuralAnnot can be used alone for the effective and efficient 3D annotation.

Figure 4 shows obtained pseudo-GTs of MSCOCO and InterHand2.6M.

#### 6.4. Comparison with state-of-the-art estimators

We show how much pseudo-GTs obtained by NeuralAnnot are beneficial by providing a comparison with recent state-of-the-art 3D human pose and mesh estimation methods using the indirect evaluation metric, introduced in Section 6.1. Table 6 shows that I2L-MeshNet trained on pseudo-GTs obtained by our NeuralAnnot significantly outperforms all previous methods, including original I2L-MeshNet trained on pseudo-GTs obtained by SMPLify-X. Table 7 shows that a regressor trained on pseudo-GTs obtained by our NeuralAnnot outperforms all previous methods on all human parts. The regressor has a simple network architecture, similar to that of ExPose [5], and its detailed description is provided in the supplementary material. Without bells and whistles, we achieved state-of-the-art performance on body-only and expressive datasets using pseudo-GTs obtained by our NeuralAnnot. This clearly shows that pseudo-GTs from our NeuralAnnot are highly beneficial for the training.

## 7. Conclusion

We present NeuralAnnot, a neural annotator that learns to construct expressive 3D human pose and mesh training



sets. Our NeuralAnnot is trained on a large number of samples in a parallel way, thus highly robust to the local minima and takes much shorter annotation time. Moreover, 3D supervisions from the auxiliary datasets decrease the depth ambiguity. The pseudo-GTs from NeuralAnnot are demonstrated to be highly beneficial as the training sets for expressive 3D human pose and mesh estimation. We will release the newly obtained pseudo-GTs of not only datasets that we used, but also other various existing 2D/3D human pose and mesh datasets, not included in the paper.

## Supplementary Material of “NeuralAnnot: Neural Annotator for in-the-wild Expressive 3D Human Pose and Mesh Training Sets”

In this supplementary material, we present more experimental results that could not be included in the main manuscript due to the lack of space.

Annotators	Err.	Time	Estimator	Metrics
<b>Human body part</b>				<b>PA MPJPE</b>
SMPLify [3]	6.9	N/A	Regressor [14, 17, 29]	85.1
EFT [12]	5.7	30 days		71.6
SMPLify-X [28]	<b>4.1</b>	6 days		79.4
SMPLify-X* [28]	<b>4.1</b>	10 days		76.7
<b>NeuralAnnot (Ours)</b>	5.2	<b>2 days</b>		<b>69.8</b>
<b>NeuralAnnot* (Ours)</b>	6.5	<b>2 days</b>		<b>68.3</b>
<b>Human hand part</b>				<b>AUC</b>
SMPLify-X [28]	<b>6.4</b>	4 days	Regressor	0.755
<b>NeuralAnnot (Ours)</b>	12.5	<b>9 hours</b>	[14, 17, 29]	<b>0.786</b>

Table 8: The 2D annotation error (pixel) and annotation time comparison between various annotators on MSCOCO and PA MPJPE comparison between a regressor trained on various pseudo-GTs of MSCOCO. The body annotators with \* output pseudo-GTs of all samples in MSCOCO, while without \* output samples only used in EFT.

## 8. Comparison with previous annotators using a different estimator

We provide an additional comparison between NeuralAnnot and previous annotators using a different estimator in Table 8. We call the estimator a regressor, which consists of ResNet and several fully connected layers. The regressor regresses human model parameters from the global average pooled ResNet output feature vector, similar to most of the previous works [14, 17, 29]. As the table shows, the regressor trained on pseudo-GTs of our NeuralAnnot achieves the best performance. The regressor has the most widely used network architecture in the model-based approach, and I2L-MeshNet, used in the main manuscript, is a state-of-the-art method model-free approach. As described in Section 2, current 3D human pose and mesh estimation methods can be categorized into model-based and model-free approaches. Therefore, the comparison validates pseudo-GTs of our NeuralAnnot are beneficial regardless of the estimator.

## 9. In-depth comparison with EFT

EFT [12] has a similar approach to ours. Unlike SMPLify-X [28], EFT is also based on a learning-based system and benefits from the 3D supervisions from the auxiliary datasets. However, there are critical differences that

make our NeuralAnnot more effective and efficient system than EFT.

- NeuralAnnot does not require sample-specific optimization in the testing stage. On the other hand, EFT performs the sample-specific optimization by minimizing 2D keypoint loss in the testing stage. This makes their testing time (several hours) much slower than ours (several minutes).
- NeuralAnnot utilizes the low-dimensional embedded pose. As Table 2 of the main manuscript shows, predicting low-dimensional pose is critical to make beneficial pseudo-GTs, especially when the samples from the target in-the-wild dataset get only the 2D supervision. However, EFT, based on SPIN [17], does not utilize low-dimensional pose, which can make their output suffer from more depth ambiguity.
- EFT require prepared SMPL fits to train a 3D human pose and mesh estimation network, and the fits are obtained by running SMPLify-X. As Table 8 shows, SMPLify-X requires long running time because of the sequential sample-specific optimization. On the other hand, our NeuralAnnot does not require any prepared fits; thus, it can provide us useful pseudo-GTs much faster than EFT.
- NeuralAnnot has a very simple architecture, thus can be easily scaled to the expressive 3D human pose and mesh. In contrast, EFT requires a well-performing pre-trained 3D human pose and mesh estimator. This is not applicable to the expressive 3D human pose and mesh estimation because only very recent methods [5] tried to address this problem.

## 10. Regressor used for EHF

The regressor used for the evaluation on EHF, shown in Table 7, has exactly the same network architecture as NeuralAnnot. There are three subnetworks for the body, hand, and face parts in the regressor. Each subnetwork consists of ResNet and several fully connected layers for the human model parameter prediction. We train each subnetwork separately, and the loss function is a  $L1$  distance between predicted and GT human model parameters and 2D/3D coordinates, similar to Kolotouros *et al.* [17]. For the final expressive 3D human pose and mesh, we integrate outputs of each subnetwork using the integration module of Section 4.4. The details of the integration module are described in Section 11.

## 11. All parts integration module

As described in Section 4.4, we selectively use global rotations of right and left hands,  $\theta_{rh}^g$  and  $\theta_{lh}^g$ , respectively,

---

**Algorithm 2** Integration of body and hands

---

**Input:**  $\theta_b^g$ : Global rotation of body

**Input:**  $\theta_b = \{\theta_j^l\}_{j=1}^{21}$ : Local rotations of body joints

**Input:**  $\theta_{rh}^g, \theta_{lh}^g$ : Global rotations of right and left hands

**Output:**  $\theta_b$ : Updated local rotations of body joints

- 1: Compute global rotations of body joints  $\{\theta_j^g\}_{j=1}^{21}$  from  $\theta_b^g$  and  $\theta_b$  by forward kinematics
  - 2: Let  $re, le, rw, lw$  denote joint index of right elbow, left elbow, right wrist, and left wrist, respectively.
  - 3: **for**  $(e, w, h) \leftarrow ((re, rw, rh), (le, lw, lh))$  **do**
  - 4:    $\theta_w^g \leftarrow \theta_h^g$
  - 5:    $x\text{-axis of } \theta_e^g \leftarrow x\text{-axis of } (\theta_e^g + \theta_h^g)/2$
  - 6:   Compute new local rotations of elbow and wrist,  $\hat{\theta}_e^l$  and  $\hat{\theta}_w^l$ , respectively, from  $\{\theta_j^g\}_{j=1}^{21}$  by reversing forward kinematics
  - 7:   **if**  $|y\text{-axis of } \hat{\theta}_w^l| < \pi/4$  and  $|z\text{-axis of } \hat{\theta}_w^l| < \pi/2$  **then**
  - 8:     Update  $\theta_w^l \leftarrow \hat{\theta}_w^l$
  - 9:     Update  $\theta_e^l \leftarrow \hat{\theta}_e^l$
  - 10:   **end if**
  - 11: **end for**
- 

when integrating outputs of networks of each part. Algorithm 2 and Figure 5 show the integration procedure and how rotations of elbow and wrist change the body, respectively. First, we perform forward kinematics to compute global rotations of all body joints, including wrists and elbows (line 1). Then, we replace the global rotations of wrists and elbows using the global rotation of hands (lines 4 and 5). The replacement assumes  $x$ -axis rotations (roll of Euler angle) of the wrist and elbow are almost the same, which follows the anatomical structure of the human body, as shown in Figure 5. To avoid a sudden change of the elbow rotation, which can cause artifacts, we use an average rotation of the elbow and wrist (line 5). From the replaced global rotations of wrists and elbows, we compute new local rotations of wrists and elbows (line 6). Finally, we check the new local rotation follows the anatomical structure of the human body (line 7), where  $y$ - and  $z$ -axis rotations are shown in Figure 5. If true, we update the local rotations of body joints, which become the final output of the integration (lines 8 and 9). We convert the 3D rotation of joints to Euler angles in line 3 - line 11.

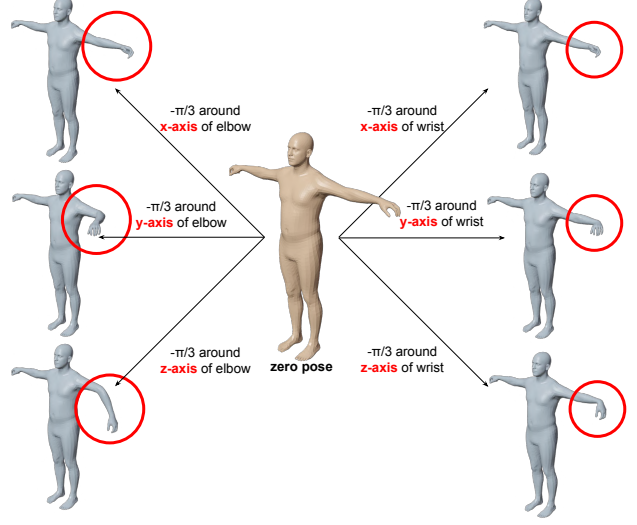


Figure 5: Visualized rotations of the elbow and wrist in each axis.

## 12. Visualization of pseudo-GTs

Figure 6 shows obtained pseudo-GTs of MSCOCO [8, 20] and InterHand2.6M [26]. Figure 7 shows pseudo-GTs from our NeuralAnnot (left) and SMPLify-X [28] (right). The figures show that our NeuralAnnot can provide accurate pseudo-GTs highly efficiently compared with SMPLify-X.



Figure 6: Visualized pseudo-GTs of MSCOCO (first to third rows) and InterHand2.6M (last row).



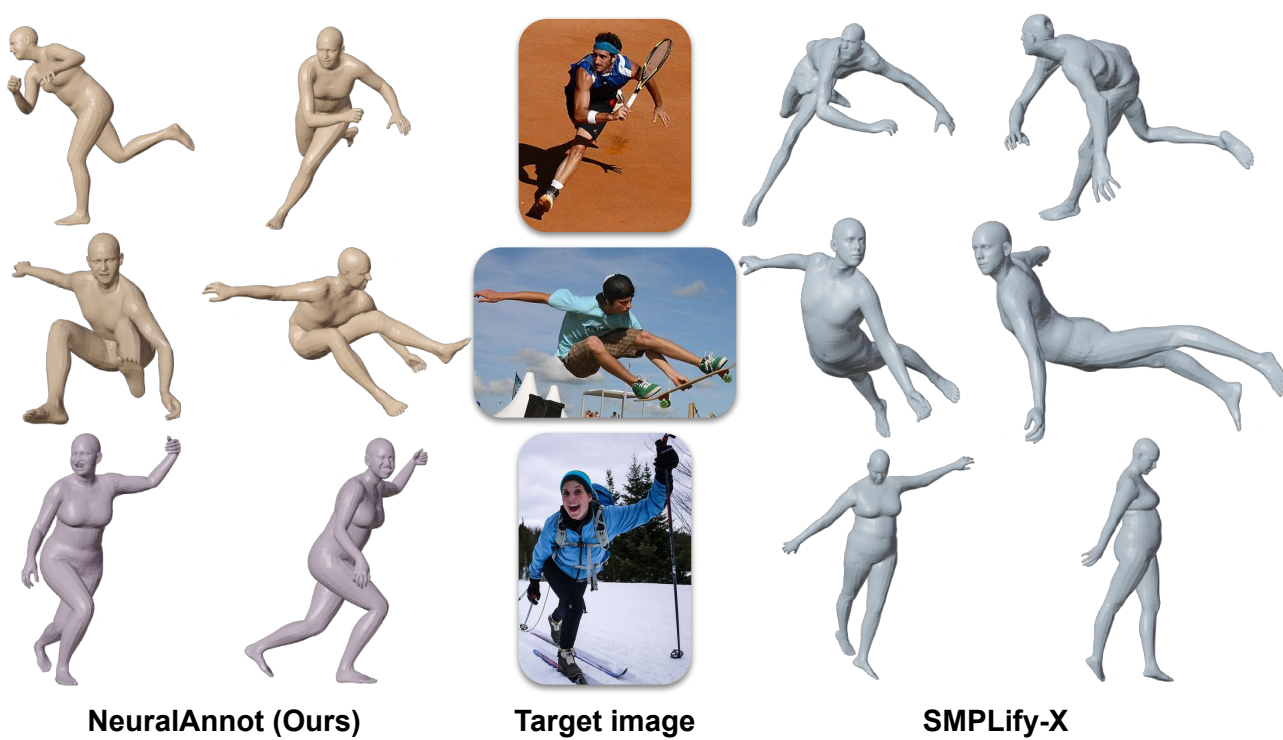


Figure 7: Pseudo-GT comparison obtained by our NeuralAnnot and SMPLify-X [28].

## References

- [1] Mykhaylo Andriluka, Umar Iqbal, Eldar Insafutdinov, Leonid Pishchulin, Anton Milan, Juergen Gall, and Bernt Schiele. PoseTrack: A benchmark for human pose estimation and tracking. In *CVPR*, 2018. 2
- [2] Mykhaylo Andriluka, Leonid Pishchulin, Peter Gehler, and Bernt Schiele. 2D human pose estimation: New benchmark and state of the art analysis. In *CVPR*, 2014. 2, 8
- [3] Federica Bogo, Angjoo Kanazawa, Christoph Lassner, Peter Gehler, Javier Romero, and Michael J Black. Keep it SMPL: Automatic estimation of 3D human pose and shape from a single image. *ECCV*, 2016. 2, 3, 6, 7, 8, 10
- [4] Hongsuk Choi, Gyeongsik Moon, and Kyoung Mu Lee. Pose2Mesh: Graph convolutional network for 3D human pose and mesh recovery from a 2D human pose. *ECCV*, 2020. 8
- [5] Vasileios Choutas, Georgios Pavlakos, Timo Bolkart, Dimitrios Tzionas, and Michael J Black. Monocular expressive body regression through body-driven attention. *ECCV*, 2020. 2, 3, 5, 8, 10
- [6] Kaiming He, Xiangyu Zhang, Shaoqing Ren, and Jian Sun. Deep residual learning for image recognition. *CVPR*, 2016. 3, 5
- [7] Catalin Ionescu, Dragos Papava, Vlad Olaru, and Cristian Sminchisescu. Human3.6M: Large scale datasets and predictive methods for 3D human sensing in natural environments. *TPAMI*, 2014. 2, 4, 5, 6, 7
- [8] Sheng Jin, Lumin Xu, Jin Xu, Can Wang, Wentao Liu, Chen Qian, Wanli Ouyang, and Ping Luo. Whole-body human pose estimation in the wild. *ECCV*, 2020. 2, 5, 6, 11
- [9] Sam Johnson and Mark Everingham. Clustered pose and nonlinear appearance models for human pose estimation. In *BMVC*, 2010. 2, 8
- [10] Sam Johnson and Mark Everingham. Learning effective human pose estimation from inaccurate annotation. In *CVPR*, 2011. 8
- [11] Hanbyul Joo, Hao Liu, Lei Tan, Lin Gui, Bart Nabbe, Iain Matthews, Takeo Kanade, Shohei Nobuhara, and Yaser Sheikh. Panoptic Studio: A massively multiview system for social motion capture. In *ICCV*, 2015. 2
- [12] Hanbyul Joo, Natalia Neverova, and Andrea Vedaldi. Exemplar fine-tuning for 3D human pose fitting towards in-the-wild 3D human pose estimation. *arXiv preprint arXiv:2004.03686*, 2020. 3, 7, 8, 10
- [13] Hanbyul Joo, Tomas Simon, and Yaser Sheikh. Total Capture: A 3D deformation model for tracking faces, hands, and bodies. In *CVPR*, 2018. 2
- [14] Angjoo Kanazawa, Michael J Black, David W Jacobs, and Jitendra Malik. End-to-end recovery of human shape and pose. *CVPR*, 2018. 2, 8, 10
- [15] Tero Karras, Samuli Laine, and Timo Aila. A style-based generator architecture for generative adversarial networks. In *CVPR*, 2019. 2, 5
- [16] Diederik P Kingma and Jimmy Ba. Adam: A method for stochastic optimization. *ICLR*, 2014. 5
- [17] Nikos Kolotouros, Georgios Pavlakos, Michael J Black, and Kostas Daniilidis. Learning to reconstruct 3D human pose and shape via model-fitting in the loop. *ICCV*, 2019. 2, 3, 6, 8, 10
- [18] Nikos Kolotouros, Georgios Pavlakos, and Kostas Daniilidis. Convolutional mesh regression for single-image human shape reconstruction. *CVPR*, 2019. 8
- [19] Tianye Li, Timo Bolkart, Michael J Black, Hao Li, and Javier Romero. Learning a model of facial shape and expression from 4D scans. *ACM TOG*, 2017. 2, 4
- [20] Tsung-Yi Lin, Michael Maire, Serge Belongie, James Hays, Pietro Perona, Deva Ramanan, Piotr Dollár, and C Lawrence Zitnick. Microsoft COCO: Common objects in context. In *ECCV*, 2014. 2, 4, 5, 6, 11
- [21] Matthew Loper, Naureen Mahmood, and Michael J Black. MoSh: Motion and shape capture from sparse markers. *ACM TOG*, 2014. 8
- [22] Matthew Loper, Naureen Mahmood, Javier Romero, Gerard Pons-Moll, and Michael J Black. SMPL: A skinned multi-person linear model. *ACM TOG*, 2015. 2, 3, 4
- [23] Dushyant Mehta, Helge Rhodin, Dan Casas, Pascal Fua, Oleksandr Sotnychenko, Weipeng Xu, and Christian Theobalt. Monocular 3D human pose estimation in the wild using improved cnn supervision. In *3DV*, 2017. 2, 4, 5, 6, 7
- [24] Dushyant Mehta, Oleksandr Sotnychenko, Franziska Mueller, Weipeng Xu, Srinath Sridhar, Gerard Pons-Moll, and Christian Theobalt. Single-shot multi-person 3D pose estimation from monocular RGB. In *3DV*, 2018. 2
- [25] Gyeongsik Moon and Kyoung Mu Lee. I2L-MeshNet: Image-to-Lixel prediction network for accurate 3D human pose and mesh estimation from a single RGB image. *ECCV*, 2020. 2, 6, 7, 8
- [26] Gyeongsik Moon, Shou-I Yu, He Wen, Takaaki Shiratori, and Kyoung Mu Lee. InterHand2.6M: A dataset and baseline for 3D interacting hand pose estimation from a single RGB image. *ECCV*, 2020. 2, 4, 5, 6, 7, 11
- [27] Adam Paszke, Sam Gross, Soumith Chintala, Gregory Chanan, Edward Yang, Zachary DeVito, Zeming Lin, Alban Desmaison, Luca Antiga, and Adam Lerer. Automatic differentiation in pytorch. 2017. 5
- [28] Georgios Pavlakos, Vasileios Choutas, Nima Ghorbani, Timo Bolkart, Ahmed AA Osman, Dimitrios Tzionas, and Michael J Black. Expressive body capture: 3D hands, face, and body from a single image. *CVPR*, 2019. 1, 2, 3, 4, 5, 6, 7, 8, 10, 11, 13
- [29] Georgios Pavlakos, Luyang Zhu, Xiaowei Zhou, and Kostas Daniilidis. Learning to estimate 3D human pose and shape from a single color image. *CVPR*, 2018. 2, 10
- [30] Javier Romero, Dimitrios Tzionas, and Michael J Black. Embodied Hands: Modeling and capturing hands and bodies together. *ACM TOG*, 2017. 2, 4
- [31] Olga Russakovsky, Jia Deng, Hao Su, Jonathan Krause, Sanjeev Satheesh, Sean Ma, Zhiheng Huang, Andrej Karpathy, Aditya Khosla, Michael Bernstein, et al. ImageNet large scale visual recognition challenge. *IJCV*, 2015. 5
- [32] Timo von Marcard, Roberto Henschel, Michael J Black, Bodo Rosenhahn, and Gerard Pons-Moll. Recovering accurate 3D human pose in the wild using IMUs and a moving camera. In *ECCV*, 2018. 2, 5, 6

- [33] Donglai Xiang, Hanbyul Joo, and Yaser Sheikh. Monocular Total Capture: Posing face, body, and hands in the wild. In *CVPR*, 2019. 2, 8
- [34] Bin Xiao, Haiping Wu, and Yichen Wei. Simple baselines for human pose estimation and tracking. In *ECCV*, 2018.
- [35] Hongyi Xu, Eduard Gabriel Bazavan, Andrei Zanfir, William T Freeman, Rahul Sukthankar, and Cristian Sminchisescu. GHUM & GHUML: Generative 3D human shape and articulated pose models. In *CVPR*, 2020. 2
- [36] Zhixuan Yu, Jae Shin Yoon, In Kyu Lee, Prashanth Venkatesh, Jaesik Park, Jihun Yu, and Hyun Soo Park. HUMBI: A large multiview dataset of human body expressions. In *CVPR*, 2020. 2
- [37] Weiyu Zhang, Menglong Zhu, and Konstantinos G Derpanis. From actemes to action: A strongly-supervised representation for detailed action understanding. In *ICCV*, 2013. 2
- [38] Yi Zhou, Connelly Barnes, Jingwan Lu, Jimei Yang, and Hao Li. On the continuity of rotation representations in neural networks. In *CVPR*, 2019. 4, 6
- [39] Christian Zimmermann, Duygu Ceylan, Jimei Yang, Bryan Russell, Max Argus, and Thomas Brox. FreiHAND: A dataset for markerless capture of hand pose and shape from single RGB images. *ICCV*, 2019. 5, 6